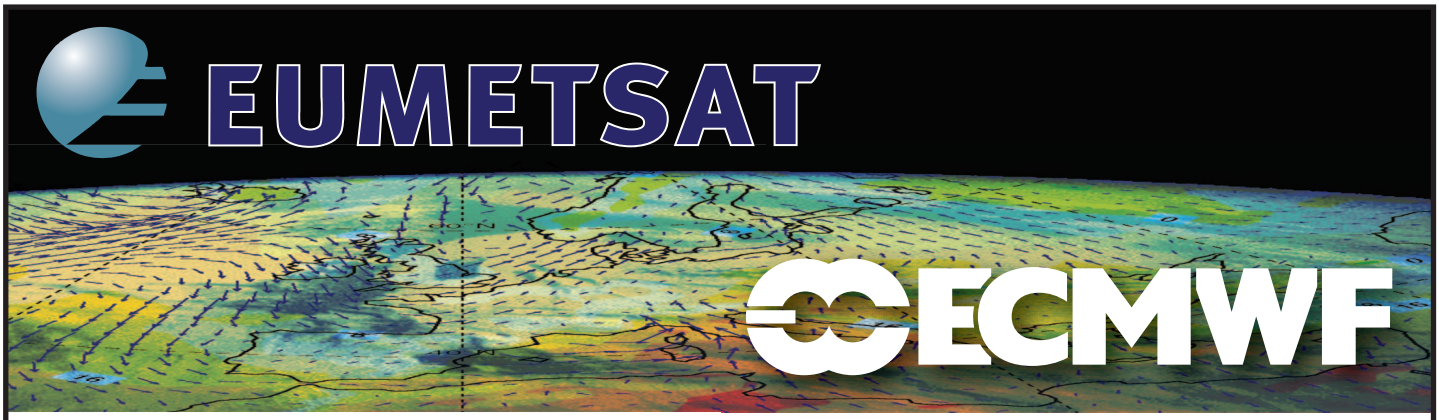

EUMETSAT/ECMWF Fellowship Programme
Research Report No. 35

New screening of cold-air outbreak regions used in 4D-Var all-sky assimilation

Katrin Lonitz and Alan Geer

February 2015

Series: EUMETSAT/ECMWF Fellowship Programme Research Reports

A full list of ECMWF Publications can be found on our web site under:
http://www.ecmwf.int/en/research/publications

Contact: library@ecmwf.int

European Centre for Medium Range Weather Forecasts
Shinfield Park, Reading, RG2 9AX, England

Abstract

In this study a new filter for biases in cold-air outbreak (CAO) regions is introduced, which is applied before assimilating microwave radiances using the all-sky approach. In cold-air outbreaks, observed microwave imager radiances are typically warmer than the corresponding model radiances. The low model radiances are believed to be caused by a higher ratio of frozen to liquid cloud water compared to what has been observed. A filter is applied to reject observations from CAO areas as the assimilation of them would degrade the analysis. The current filter also rejects some unbiased microwave imager/sounder radiances, whereas the new filter identifies CAO areas more precisely using predictors of stability and the ratio between liquid and total cloud water. Using the new filter increases the amount of microwave imager data by $\sim 1.5\%$ in the winter hemisphere, which corresponds to $\sim 0.4\%$ globally. This has a neutral impact on the forecast scores for humidity, temperature and wind, proving that the new filter works well in detecting systematically biased data from CAO regions while rejecting less unbiased data.

1 Motivation

Microwave imager radiances in clear, cloudy and rainy conditions (also known as all-sky conditions) have been assimilated operationally into the ECMWF numerical weather prediction (NWP) system since 2009 (Bauer et al. [2010], Geer et al. [2010]). Currently, observed radiances within a 12-hour window and frequencies between 19 and 90 GHz from the microwave imagers Special Sensor Microwave Imager/Sounder (SSMI/S) and TRMM Microwave Imager (TMI) are assimilated actively with a four dimensional variational scheme (4D-Var) Rabier et al. [2000]. In the next operational cycle, also sounding channels at 183 GHz from Microwave humidity sounders (MHS) and SSMI/S are assimilated with the all-sky approach (Geer et al. [2014]). That means, in order to fit features of cloud and precipitation observed within the microwave, 4D-Var has to adjust cloud and precipitation next to moisture and dynamical fields (e.g. wind).

The assimilation of some microwave observations is, however, not beneficial for the quality of the analysis (see chapter 2). Observations in 'cold-air-outbreak' (CAO) areas have a large systematic bias between model and observations. Microwave observations in these CAO areas are filtered out in the current configuration of the IFS (40r1). However, the filter is not optimal as observations which are not affected by cold-air outbreaks are filtered out, too. In this study, we introduce a new CAO filter which allows more microwave data to be assimilated and helps to identify the biased areas more precisely using the physically-based stability predictor.

2 All-sky assimilation system

The assimilation of cloudy and rainy radiances is non-trivial and has to be done carefully in order to avoid a degradation in the quality of the analysis. For example, radiances can exhibit non-Gaussian behaviour (e.g Errico et al. [2007]) which, if assimilated, would disobey one of fundamental assumptions in 4D-Var. Geer and Bauer [2011] introduced a symmetric error model to overcome the non-Gaussianity of cloudy and rainy radiances. In order to obtain an (almost) Gaussian error distribution they identified the dependence of the First Guess (FG) standard deviation on the mean cloud amount and used it to normalise FG departures.

This new observation error formulation takes also into account that errors are higher in cloudy and rainy situations than in clear skies. Because of the high errors the assimilation of rainy and cloud radiances

have a smaller impact on the analysis than the assimilation of clear sky radiances. However, the new observation error formulation is more realistic than in the initial all-sky implementation (Bauer et al. [2010], Geer et al. [2010]), where very high observation errors have been applied to cloudy and rainy radiances. Other sources of error are based in the model itself as it has larger forecast errors for cloud and precipitation fields than for dynamical variables such as temperature. Furthermore, the observation operator in the microwave, RTTOV-SCAT (Bauer et al. [2006]), includes many assumptions (e.g. cloud overlap, fall speed of hydrometeors, hydrometeor size distribution) and is, therefore, prone to errors.

A good knowledge of these errors is important to be able to estimate the accuracy of the forecast model and observation operator, which is crucial for the quality of the analysis. The quality or rather the suitability of the observed microwave data is also essential. That means for example, microwave imager observations are only assimilated between 60°S and 60°N over ice-free oceans and microwave soundings all over the globe over land, ocean and sea ice except over mid to high orography. A first guess (FG) check and a Variational Quality Control (VarQC; Ingleby and Lorenc [1993], Anderson and Järvinen [1999]) also controls the quality of observations. The former, applies a threshold check of departures whereas the latter reduces the weight of observations which differ significantly from the main analysis.

To remove systematic biases between model and observations the Variational Bias Correction (VarBC; Dee [2004], Auligné et al. [2007]) is used. To estimate biases a parameter, which is globally constant, is added to a linear function of different sets in bias predictors, depending on the instrumental data assimilated. For example, for SSMIS those bias predictors are skin temperature, total column water vapour (TCWV), surface wind speed and a third-order poly-nominal in instrument scan position. However, there is not yet a correction for cloudy and rainy biases because they are highly situation dependent, i.e. it is difficult to find an appropriate predictor. In the near future some work will be done trying to identify causes of global biases (caused by model or observation operator) in cloudy and rainy situations. But for situation dependent biases, e.g. in cold-air outbreak areas, the best solution is still to screen out the data.

3 Filter in cold-air outbreak areas

Cold-air-outbreak areas occur in the winter in high latitudes, where cold dry air is advected over the relative warm ocean forming shallow convective clouds. An example of cold-air-outbreak areas is shown in Fig. 1 where the CAO area is marked by open convection and low temperatures below freezing point (see red circled area).

Fig. 2 shows a CALIPSO data cross section for this example of retrieved cloud phase. Clouds in the CAO area (between 60°S/117°W and 27°S/127°W) have liquid water at cloud top, which is different to the modeled water phase of those clouds. In CAO areas the model tends to produce too much ice compared to observations, which show often liquid-phase clouds even though temperatures are far below freezing point. The corresponding model fields for the CAO area discussed in Fig. 3, where the lack of modeled cloud liquid water is visible. Work to address this model problem is ongoing in the ECMWF's Physical Aspects section by Richard Forbes. As long as this systematic bias is existent, a screening of observed data in CAO areas is necessary. This is because the data assimilation (DA) system cannot compensate for model biases. That means, if one assimilates data in areas with a systematic bias the assumptions made in DA are violated and the performance of the DA system is not optimal.

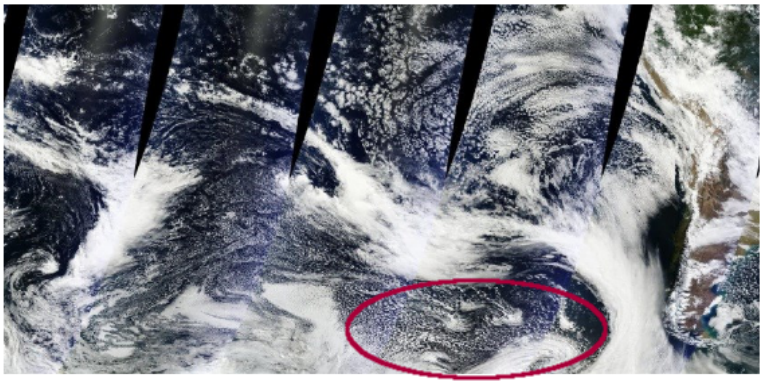

Figure 1: Composite MODIS image on 24 August 2013 at 08 Z, showing a cold-air outbreak area (circled in red) with flow from Antarctica over ocean and increasing convective cloud development. The whole area shown spans from 180°W to 60°W and from the equator to 60°S.

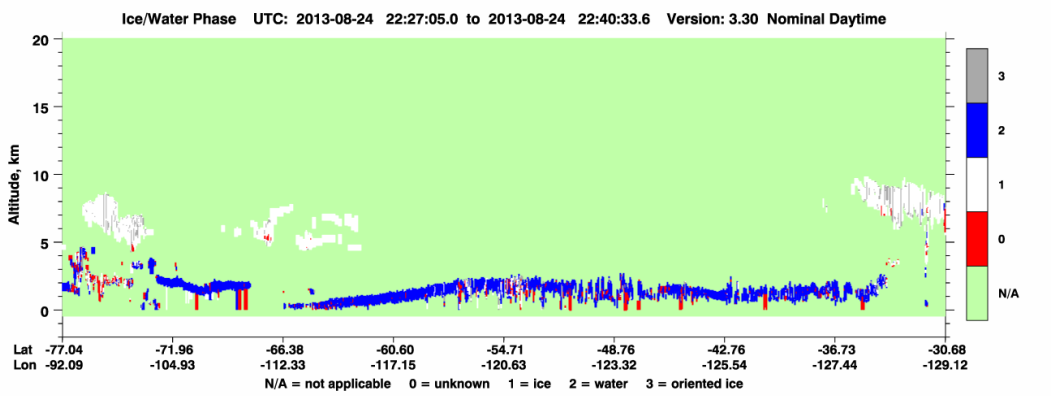

Figure 2: CALIPSO data cross section on 24 August 2013 at ∼ 22Z of retrieved cloud phase. The x-axis shows the location (lat/lon). The colours refer to the water phase (red = unknown, white = ice, blue = water, grey = oriented ice). Most of the low cloud has liquid water at cloud top. (source: http://www-calipso.larc.nasa.gov/products/lidar/browse_images/show_date.php?s=production&v=V3-30&browse_date=2013-08-24)

In the past, CAO areas have been screened out by the following criteria (Geer and Bauer [2010]):

$$\begin{aligned} \mathrm{TCWV} &< 15\,\mathrm{kg\,m^{-2}}, \\ \frac{\mathrm{LWP}}{\mathrm{LWP}+\mathrm{IWP}} &< 0.5, \\ \mathrm{LWP}+\mathrm{IWP}+\mathrm{RWP}+\mathrm{SWP} &> 0.01\,\mathrm{kgm^{-2}}, \end{aligned} \tag{1}$$

with modeled total column water vapour (TCWV), cloud liquid water path (LWP), cloud ice water path (IWP), rain water path (RWP), and snow water path (SWP). This screening was efficient enough to filter out biased CAO areas, however, unbiased areas were also filtered out. We refer to this filter as "filter1".

In September 2011 another filter, which we will refer to "filter 2", was added in CAO- and other areas with very low water vapour content in cycle 37r3:

$$\mathrm{TCWV} < 8\,\mathrm{kg\,m^{-2}}. \tag{2}$$

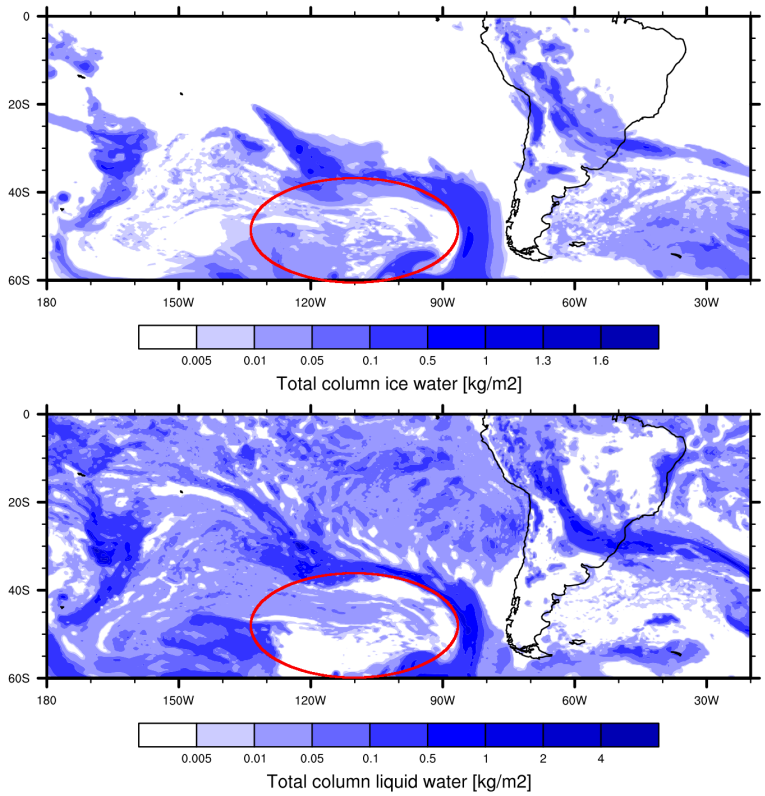

Figure 3: Model fields from cycle 40r2 on 24 August 2013 at 12Z. In the red circle the observed CAO area, displayed in Fig. 1 is highlighted. Top panel: modeled total column ice water [kg m^{-2}]. Bottom panel: modeled total column liquid water [kg m^{-2}].

The reason for the implementation of filter 2 was an issue in the assimilation system, which started to generate large negative temperature increments at high latitudes with near-zero TCWV in the lower troposphere over ocean. This behaviour was triggered by 37r3 model changes to supersaturation and deposition rate for clouds, which were necessary to fix a 2m-temperature bias in winter. In general the liquid cloud amount was increased, however, for areas south of 45°S this resulted into higher LWP in the stratiform cloud regime under conditions with very low water vapour; eventually causing negative temperature increments. For more details see Geer et al. [2011].

The current CAO filter applies to microwave imager data over ocean, which are assimilated using 4D-Var all-sky (e.g. Bauer et al. [2010], Geer et al. [2010]). However, for cycle 41r1 of the Integrated Forecast System (IFS) data over ocean from microwave sounders are additionally affected by this filter comprising a total of data from one Special Sensor Microwave Imager/Sounder (SSMIS) on board of DMSP-17, one TRMM Microwave Imager (TMI) on-board of TRMM and four Microwave Humidity Sounders (MHS) on-board of NOAA-18, NOAA-19, METOP-A and METOP-B (for 183 GHz only 183 $\pm$7 GHz is affected by the filter, neither 183$\pm$1 GHz nor 183$\pm$3 GHz). We will refer to them as “all-sky instruments”.

4 Description of new filter

In this study, we introduce a new filter instead of the old filter 1 in order to increase the number of unbiased microwave imager data in the all-sky system. Originally, we intended to omit the use of filter 2, but results showed that assimilating low TCWV regions still causes a degradation in forecast scores. Hence, it was decided to use a combined version of a new filter 1 and the old filter 2. Nevertheless, investigations on low TCWV areas are ongoing.

The new filter 1 uses a combination of the atmospheric stability and the ratio of liquid to total cloud water. A study by Kazumori et al. [2014] inspired the use of a stability measure in CAO areas. They found negative correlation between First Guess (FG) departures and the air-sea temperature difference at high wind speeds ($> 10\ \mathrm{m\,s^{-1}}$) for different frequencies of Advanced Microwave Scanning Radiometer 2 (AMSR2). Their results show that under cloudy conditions positive biases in brightness temperature (Tb) occur which are even higher when the surface wind speed is increased. Under high surface wind speed conditions the sea produces foam and whitecaps, as argued by Kazumori et al. [2014]. A surface emissivity model which takes this phenomenon into account would reduce high biases in Tb for high wind speeds. However, that is a small part of the bias at frequencies assimilated (e.g. 19 - 183 GHz). The main bias is very likely the lack of water clouds in unstable areas. The new filter 1 uses this behaviour of stability (temperature difference) as one measure to detect CAO areas, next to the cloud water phase information. Hence, the new filter 1 is physically more consistent with the nature of CAO areas than the old filter 1.

That means, the new filter 1 screens out cold-air outbreak areas under the following criteria:

$$\begin{aligned} \mathrm{LTS} &< 12\,\mathrm{K}, \\ \frac{\mathrm{LWP}}{\mathrm{LWP}+\mathrm{IWP}} &< 0.5, \end{aligned} \tag{3}$$

using lower tropospheric stability (LTS), which is simply the difference in potential temperature (Θ) between the 700 hPa pressure level and the surface (Klein and Hartmann [1993]). It can be seen as a measure of the strength of the inversion that caps the planetary boundary layer and is, therefore, a good measure for the stability in this layer. Conditions in cold-air outbreak areas are affected by cold dry air above a warmer sea surface, which means the air is very unstable and, hence, the LTS is rather low; smaller than 12 K. That suggests that using stability as a predictor to filter out CAO areas is more precise than the old filter.

However, a second condition in (3) is still necessary to select only biased CAO conditions where the model produces too much ice cloud water instead of liquid cloud water. If model cloud physics will be capable of addressing the bias in CAO areas in the future, one has to reassess if the filter 1 is still necessary and if so, think about adjustments of the second condition in the new filter.

Fig. 4 shows which areas are identified as CAO areas by the new filter 1 compared to the old filter 1. Areas of cold air outbreaks show typically high positive FG departures, that means the modeled brightness temperatures are lower than the observed ones. This is most probably caused by the model's inability to produce enough cloud liquid water. Instead, the model shows too much ice-phase clouds in CAO areas. Cloud ice is almost transparent at 37 GHz whereas liquid water absorbs and emits it. That means brightness temperatures increase with an increase in the amount of liquid water, but show little response to an increase in the amount of ice. The lower the amount of modelled liquid water the lower the model brightness temperature in 37 GHz and the higher are positive FG departures in areas where observations show mostly clouds with a liquid-phase, as they do in CAO areas.

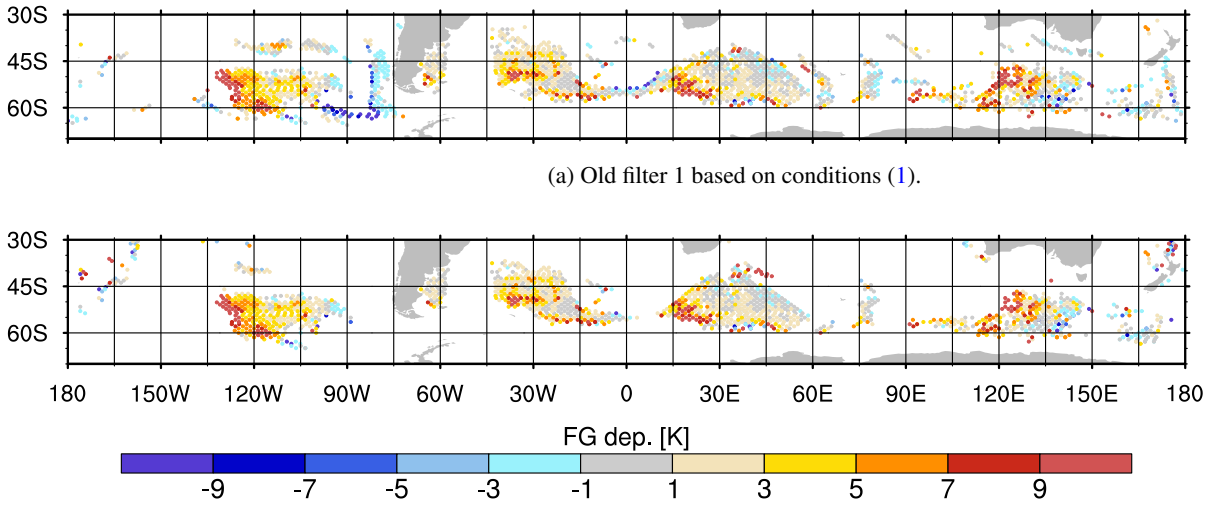

(a) Old filter 1 based on conditions (1).

(b) New filter 1 based on conditions (3).

Figure 4: FG departures from SSMIS-F17 in channel 16 (37 GHz, vertical polarisation) for identified CAO areas between 30°S and 80°S in the 12 Z model cycle of 24 August 2013.

Areas with small or negative FG departures in high latitudes can, therefore, be seen as areas free of cold-air outbreaks. That means the grey and perhaps blue (certainly they are not CAO areas) coloured areas in Fig. 4a are areas without a systematic model bias, which are wrongly identified as biased CAO areas using the old filter 1. One can easily see that the number of these areas is reduced in Fig. 4b, showing CAO areas identified with the new filter 1. In chapter 5 the increase in number of actively assimilated data are presented for the different all-sky instruments.

5 Results

In order to investigate the performance of the new filter for CAO areas (new filter 1 + old filter 2, see chapter 3) with the original filter (old filter 1 + old filter 2) we run several data assimilation experiments using the 41r1 cycle of Integrated Forecast System (IFS). Experiments include different combinations or turning off filter 1 and filter 2. For clarity, only results of two experiments are shown, one with the original filter (oldf1, oldf2) and one with the new filter (newf1, oldf2). The experiments have been run for the period between 1 July 2013 and 30 September 2013 with a model resolution of T511 and 137 vertical levels.

Experiments utilising the new CAO filter and having modifications to the usage of other satellite data have been run over six months (1 February to 30 April 2014 and 1 June to 31 August 2014) with cycle 41R1 and a resolution of T639 and 137 vertical levels. Results from these experiments are qualitatively consistent with results from the experiments discussed in this report, which strengthens the conclusion about the new CAO filter in ch. 6.

5.1 First guess departures

It is interesting to see if the new filter is more efficient in detecting CAO areas than the original filter. For this reason, the mean in normalised FG departures (FG departure divided by the observation error) is calculated for both filters over a time period between 1 July 2013 and 30 September 2013 (see Fig. 5). The patterns of normalised FG departures of the original filter and the new filter look very similar which indicates that both filters identify similar areas as CAO areas. However, the difference in the normalised FG departures reveals that the new filter allows FG departures to attain slightly higher values in the high latitudes of the southern hemisphere where also CAO areas could potentially be found for this time period. Analysis shows that this behaviour stems from regions with negative FG departures, which are regions not affected by the typical CAO bias (see top two panels of Fig. 5). Here, the new filter causes a reduction of high negative normalised FG departures. Sampling only regions with positive FG departures, which could potentially be non-detected CAO areas, reveals no difference in normalised FG departure in the high latitudes in the southern hemisphere, implying that the new filter works at least as efficient as the original filter. Also the positive change in FG departures counteracts the negative bias in Fig. 5a) and Fig. 5b) in those areas.

5.2 Forecast errors

By using the new filter we expect that the number of unbiased observations of all-sky instruments (see chapter 4) increases. Forecast scores are not expected to change much, as the affected number of observations is a small proportion of the total. In fact, this behaviour can be found for relative humidity (RH), in small but insignificant changes throughout the atmosphere in the root mean square (RMS) in forecast error (forecast - analysis) for the whole forecast period (Fig. 6).

A slight reduction ($\sim$ 4%) of the RMS error in relative humidity has been noticed in the stratosphere around 5 hPa (not shown). This feature of improved forecast scores seem to occur persistently in a single model level throughout the forecast range of 10 days. Recently, it has been observed in other assimilation/model experiments as well. Because of the small change in magnitude and its appearance in other experiments, we think these stratospheric changes are not significant for the evaluation of the new CAO filter.

The forecast scores, in terms of RMS forecast errors and anomaly correlation, do not differ significantly for horizontal wind, geopotential height (both not shown), and temperature (Fig. 7). Here, the differences in the RMS forecast error are within the confidence range in all geographical regions and pressure levels. That means the new filter works in terms of allowing more microwave data assimilated through the all-sky path without degrading the forecast scores.

5.3 Fit and Usage of observations

As mentioned before, the screening of cold-air outbreaks only applies to data assimilated using the all-sky approach. Hence, only the number of actively assimilated data from e.g. SSMIS and MHS should be increased when using the new filter. In Fig. 8b it is shown that the number of SSMSI-F17 data for microwave channels is increased by $\sim$ 1.5 % in the southern hemisphere, but only by $\sim$ 0.4 % globally. This is because CAO areas occur predominately in the winter hemisphere. In the southern hemisphere this would be May to September, in which the experiment time is embedded. That means the highest increase in number of microwave observations can be seen in the southern hemisphere for this experiment

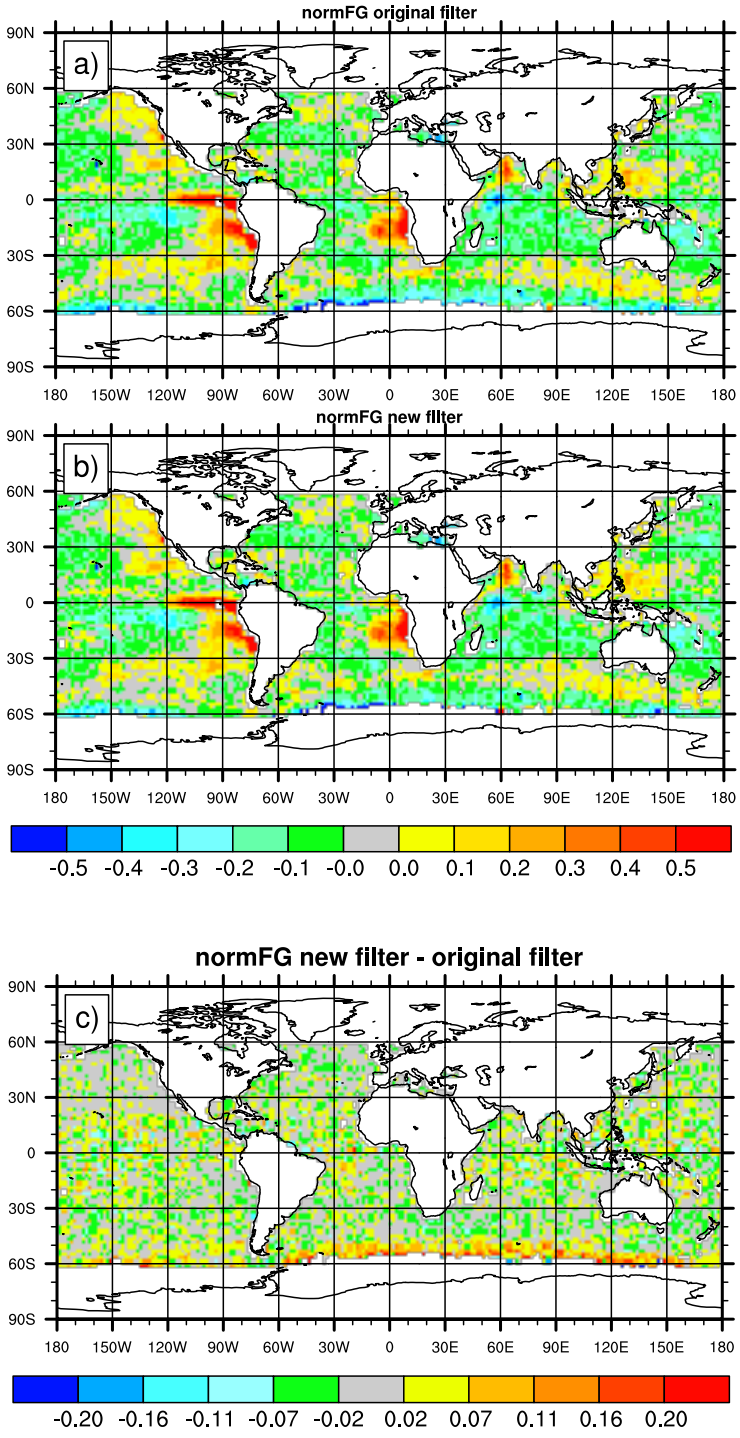

Figure 5: Mean in normalised First Guess departure (FG departure divided by observation error) from runs with a) the original filter, b) the new filter and c) the difference in normalised FG departure between new and original filter over a time period between 1 July 2013 and 30 September 2013. The mean in normalised FG dep. is calculated for every 2° latitude × 2° longitude box.

setup. Similar numbers can be found also for MHS (not shown). Simultaneously, the standard deviation in FG departure (Fig. 8a) is reduced for microwave channels because the relative number of low FG departure observation is increased. However, there is no change for SSMIS channels 10 and 11 (183 ± 3 GHz and 183 ± 1 GHz, respectively) as seen in Fig. 8b. The reason is that these sounding channels are not actively assimilated using the all-sky approach (see chapter 3), i.e. the new filter is not applied.

To judge the effect of the new filter on the behaviour of the assimilation of other instruments, for which the number of actively assimilated data is hardly affected by the new filter 1, FG departures of different satellite observations are analysed. Fig. 9 shows the normalised standard deviation in Analysis and FG departures of humidity observations from the Advanced Microwave Sounding Unit [AMSU-A] (Fig. 9a), humidity and temperature observations from the Infrared Atmospheric Sounding Interferometer [IASI] (Fig. 9b), and wind observations from various satellite platforms [SATOB] (Fig. 9c) in the southern hemisphere. The differences of the standard deviation in FG departure between the two experiments: original filter and new filter is within the confidence range for all displayed instruments. Also, globally the FG departures vary within the confidence range (not shown). That means the usage of the new filter impacts the statistics of other actively assimilated instruments neutrally.

6 Summary

A new filter for cold-air outbreak (CAO) areas has been introduced, which identifies CAO more precisely based on their physical characteristics.

Applying a filter in CAO areas is necessary because a systematic bias exists here between the model and microwave imager/sounder observations. The assimilation system cannot cope with systematic biases and, hence, observations in these regions have to be filtered out before being assimilated. If assimilated, the use of these observations would degrade the analysis. The bias in CAO seems to stem from a deficiency of the model in representing the phase of the clouds in CAO regions correctly. Even though temperatures are far below freezing point, observations (e.g. with CALIPSO) detect liquid cloud droplets, whereas the model produces mostly ice-phase clouds. In the future it is hoped to solve this model deficiency, which would make the filter in CAO areas redundant. Work is ongoing in the Physical Aspect Section at the ECMWF, but until this systematic bias is eliminated a filter is necessary.

The current filter uses a combination of predictors on the information of total water, cloud water phase and water vapour to identify CAO regions. Unfortunately, some unbiased data is rejected with this filter, too. Predictors, such as stability and the cloud water phase information make the new filter much better in retaining more unbiased microwave data while still being able to identify systematic biased areas of CAOs. In fact, the number of actively assimilated microwave imager data from SSMIS is increased by $\sim 1.5\%$ in the southern hemisphere ($\sim 0.4\%$ globally), when the new filter is used. The more targeted identification of CAO regions is most likely caused by the stability predictor in the new filter. As mentioned before, the lower atmosphere is quite unstable in cold-air outbreak events. That means the stability criterion is much more physically based compared to information about total water and water vapour and is, hence, more targeted in the identification of CAO areas.

However, one cannot expect that such a small number of additional microwave data would improve significantly the forecast scores. Investigations of forecast scores and FG departures from various satellite instruments, which are sensitive to wind, humidity and temperature, show that the new filter affects neutrally the quality of the analysis. Being able to use more observations and not degrade the analysis supports the use of the new cold-air outbreak filter.

Acknowledgements

Katrin Lonitz's work at ECMWF is funded by the EUMETSAT fellowship programme. The authors would also like to thank Richard Forbes for fruitful discussions.

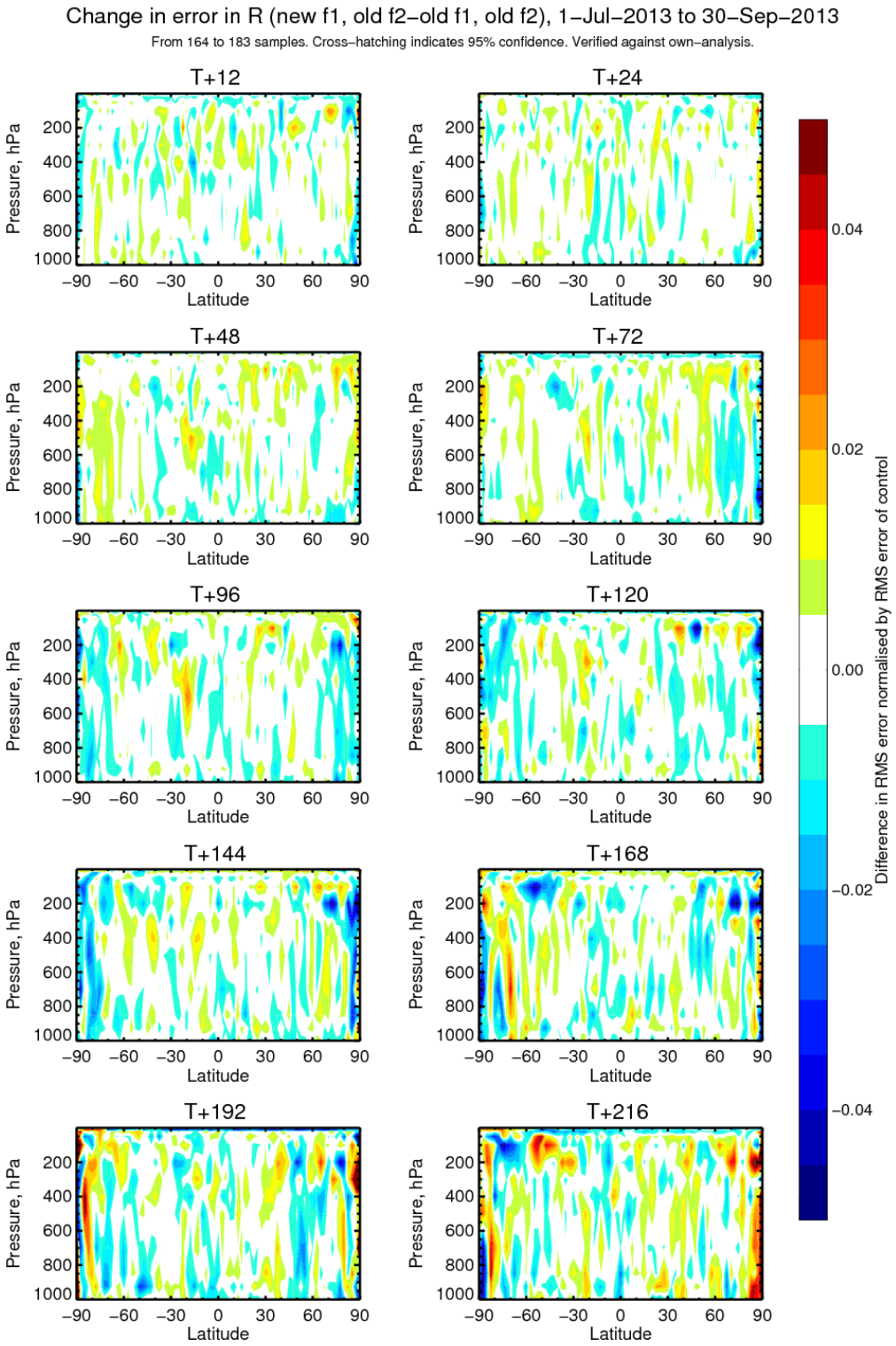

Figure 6: Difference in relative humidity RMS error normalised by RMS error of control (oldf1, oldf2). Blue colours correspond to an improvement in forecast scores and red colours correspond to a degradation in forecast scores. Significant differences are hatched.

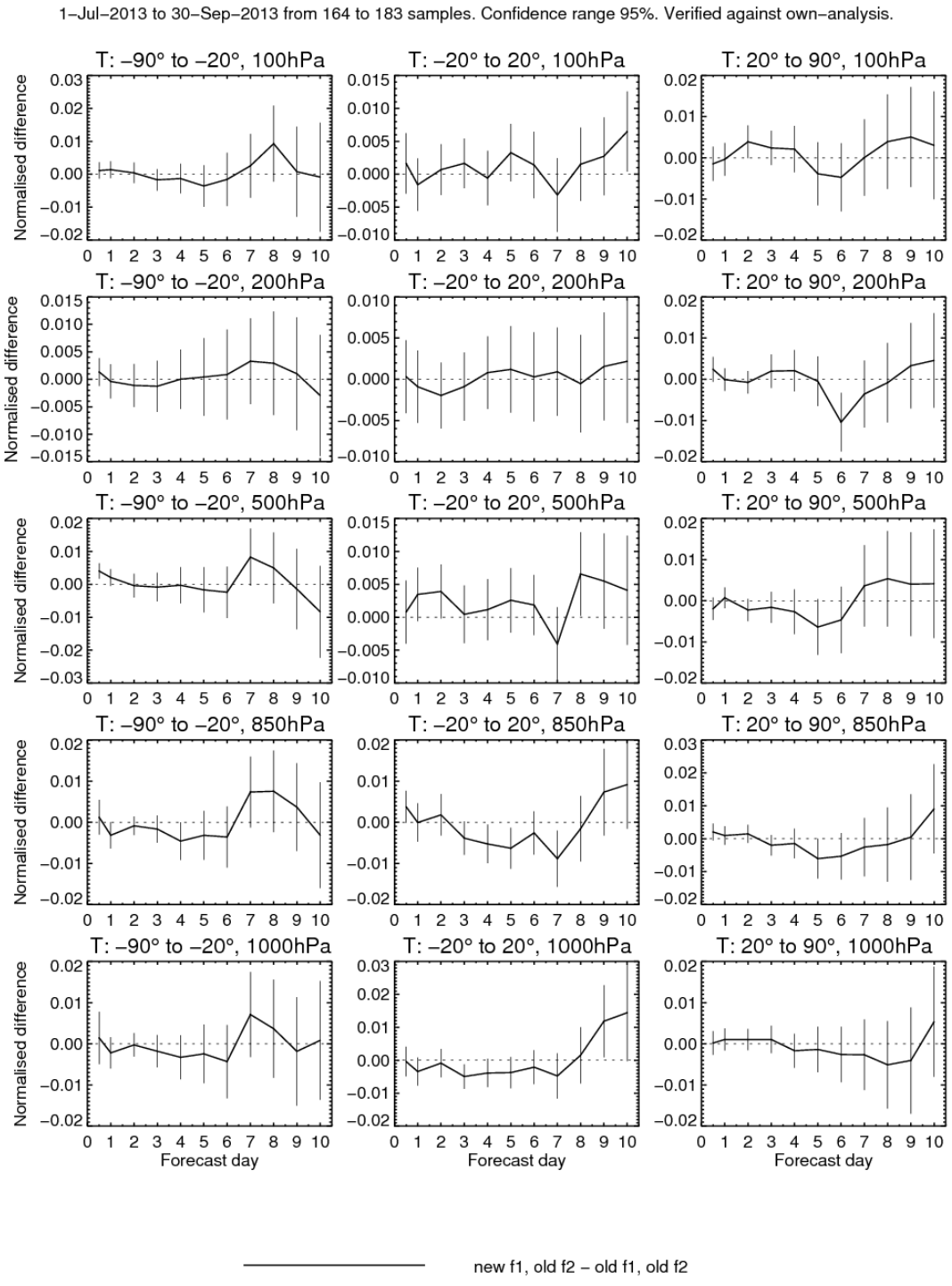

Figure 7: Difference in temperature RMS error normalised by RMS error of control (oldf1, oldf2) as a function of forecast day for different geographical regions and pressure levels. Negative values correspond to an improvement in forecast scores and positive values correspond to a degradation in forecast scores. The confidence range is displayed by vertical bars.

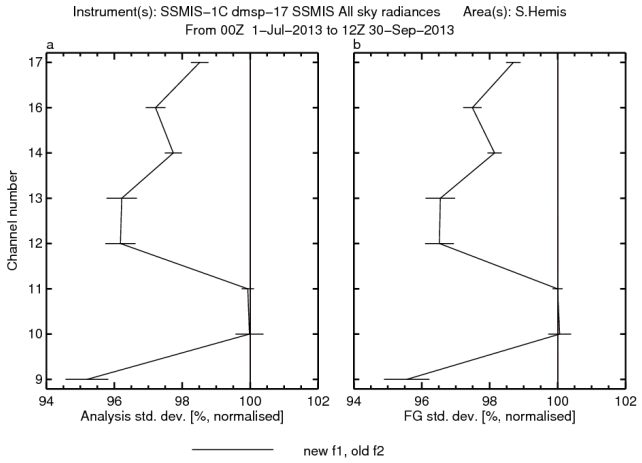

(a) Standard deviation in FG and analysis departures normalised by control.

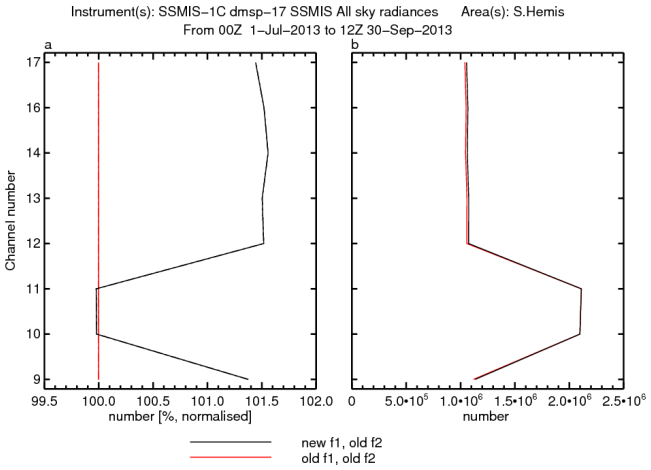

(b) Number of actively assimilated data.

Figure 8: Standard deviation in FG/AN departures and number of actively assimilated data from SSMIS-F17 for different channels in southern hemisphere. Confidence ranges are displayed by horizontal bars per channel.

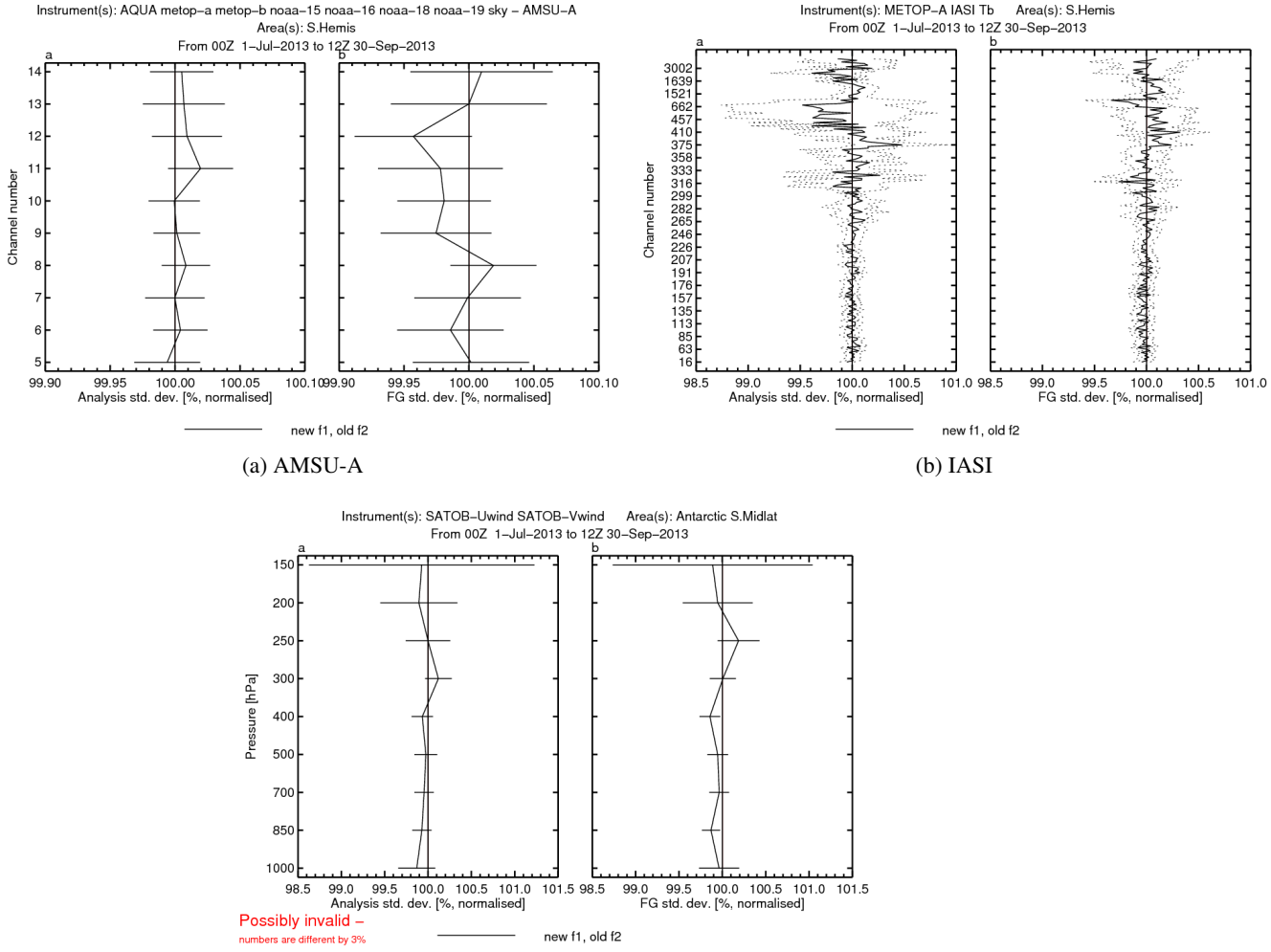

(a) AMSU-A

(b) IASI

(c) SATOB

Figure 9: Standard deviation in FG/AN departures from a) Advanced Microwave Sounding Unit [AMSU-A] instruments, b) Infrared Atmospheric Sounding Interferometer [IASI] and c) wind observations from various satellite platforms [SATOB] for different channels in southern hemisphere. Confidence ranges are displayed by horizontal bars per channel.

References

P. Bauer, A. Geer, P. Lopez, and D. Salmond. Direct 4D-Var assimilation of all-sky radiances. Part I: Implementation. *Q.J.R. Meteorol. Soc.*, 136(652):1868–1885, 2010.

A. Geer, P. Bauer, and P. Lopez. Direct 4D-Var assimilation of all-sky radiances. Part II: Assessment. *Q.J.R. Meteorol. Soc.*, 136(652):1886–1905, 2010.

F. Rabier, H. Jäervinen, E. Klinker, J.-F. Mahfouf, and A. Simmons. The ECMWF operational implementation of four-dimensional variational assimilation. I: Experimental results with simplified physics. *Q.J.R. Meteorol. Soc.*, 126(564):1143–1170, 2000.

A. Geer, F. Baordo, N. Bormann, and S. English. All-sky assimilation of microwave humidity sounders. *ECMWF Tech. Memo.*, 741, 2014.

R. Errico, P. Bauer, and J.-F. Mahfouf. Issues regarding the assimilation of cloud and precipitation data. *J. Atmos. Sci.*, 64(11):3785–3798, 2007.

A. Geer and P. Bauer. Observation errors in all-sky data assimilation. *Q.J.R. Meteorol. Soc.*, 137(661): 2024–2037, 2011.

P. Bauer, E. Moreau, F. Chevallier, and U. O'Keeffe. Multiple-scattering microwave radiative transfer for data assimilation applications. *Q.J.R. Meteorol. Soc.*, 132(617):1259–1281, 2006.

N. Bruce Ingleby and A. Lorenc. Bayesian quality control using multivariate normal distributions. *Q.J.R. Meteorol. Soc.*, 119(513):1195–1225, 1993.

E. Anderson and H. Järvinen. Variational quality control. *Q.J.R. Meteorol. Soc.*, 125(554):697–722, 1999.

D. Dee. Variational bias correction of radiance data in the ECMWF system. *Proceedings of workshop on assimilation of high spectral resolution sounders in NWP*, ECMWF, Reading UK, 28 June – 1 July 2004:97–223, 2004.

T. Auligné, A. McNally, and D. Dee. Adaptive bias correction for satellite data in a numerical weather prediction system. *Q.J.R. Meteorol. Soc.*, 133(624):63i–642, 2007.

A. Geer and P. Bauer. Enhanced use of all-sky microwave observations sensitive to water vapour, cloud and precipitation. *ECMWF Tech. Memo.*, 620, 2010.

A. Geer, R. Forbes, P. Bauer, and F. Baordo. Big temperature increments in the 37r3 esuite coming from all-sky observations in the southern winter. *ECMWF Research Dep. Memo.*, R43.8/AG/11110, 2011.

M. Kazumori, A. Geer, and S. English. Effects of all-sky assimilation of GCOM-W1/AMRS2 radiances in the ECMWF system. *ECMWF Tech. Memo.*, 732, 2014.

S. Klein and D. Hartmann. The seasonal cycle of low stratiform clouds. *J. Climate*, 6(8):1587–1606, 1993.